Acta Cryst. (1998). D**54**, 1216–1229

Polarized Raman Spectroscopic Studies of Tetragonal Lysozyme Single Crystals

A. B. Kudryavtsev,[a]* S. B. Mirov,[a] L. J. DeLucas,[b] C. Nicolete,[b] M. van der Woerd,[b] T. L. Bray[b] and T. T. Basiev[c]

[a]*The University of Alabama at Birmingham, Department of Physics, 310 Campbell Hall, 1300 University Boulevard, Birmingham, AL 35294-1170, USA,* [b]*The University of Alabama at Birmingham, Center for Macromolecular Crystallography, Birmingham, AL 35294-1170, USA, and* [c]*General Physics Institute, Russian Academy of Sciences, Moscow 117942, Russia. E-mail: akudryav@phys.uab.edu*

(*Received 15 September 1997; accepted 22 January 1998*)

Abstract

Polarized Raman spectra have been obtained for tetragonal lysozyme single crystals of different relative quality. The Raman band at 507 cm^{-1}, which corresponds to the totally symmetric stretch vibration of the *gauche-gauche-gauche* (ggg) disulfide bridges of the protein, has been shown to possess different polarization characteristics compared with the *gauche-gauche-trans* (ggt) disulfide bridge band at 528 cm^{-1}. The relative intensities of the ggg and ggt bands in the polarized Raman spectra have been numerically estimated for a number of tetragonal lysozyme single crystals, the X-ray diffraction data of which are available from the Protein Data Bank. On the basis of comparison between the experimental and calculated polarization characteristics of the disulfide Raman lines, the following main conclusions have been drawn. The orientation of the protein molecules correlates with the average orientation of their ggg disulfide bridges. This in turn can be described by the ρ_{ggg} value which reflects the average orientation of the S—S bonds with respect to the Z crystallographic axis and can be determined from polarized Raman spectra. Crystals of better quality are characterized by a better alignment of the protein molecules with respect to the Z axis, a smaller perturbation of the protein molecules in the crystal lattice and a somewhat higher interlattice water content.

1. Introduction

The main goal of this work was to explore the suitability of using laser Raman spectroscopy as a non-destructive non-invasive technique for the measurment of the quality of protein crystals. As an object for this study, we selected tetragonal hen egg-white lysozyme single crystals (TLSC), the most comprehensively studied protein crystals.

The crystal-lattice order is reflected in Raman spectra predominantly in the region of external (lattice) vibrational modes which are located in the low-frequency part of the spectrum. For inorganic crystals the lattice modes are usually located in the frequency range 20–400 cm^{-1}. The sharper Raman lines corresponding to the lattice vibrational modes (high intensity and narrow linewidth) *i.e.* those with a high number of each type of lattice phonon and a longer lifetime, should indicate a greater extent of crystal lattice ordering and perfection. Unfortunately, this simple approach did not prove to be very effective in the present investigations. Because of the high molecular weight and moment of inertia of the lysozyme molecules and their weak intermolecular bonding compared with inorganic molecular crystals, the frequencies ν_L of the lattice vibrational modes should be small [roughly $\nu_L \simeq (k/M)^{1/2}$, where k is the intermolecular bond force constant and M is the molecular mass]. Genzel *et al.* (1976), with the aid of special experimental techniques, have monitored a Raman line of frequency 25 cm^{-1} in a lysozyme crystal, which was absent from the spectrum of a lysozyme solution in water. They reasonably assigned the origin of this line to the lattice vibrational motion. Unfortunately, in the present study, we were not able to register Raman lines with frequencies less than 200 cm^{-1}. Our approach is based on the fact that the extent of the crystal-lattice ordering may be defined from the Raman spectra of the internal molecular vibrations, which reflect the intermolecular alignment, thus serving as a spectroscopic probe of crystal ordering and perfection. Here the protein subgroups located near to protein–protein contacts make the main contribution. The Raman lines of the internal molecular vibrations may be shifted, split or broadened when long-range Coulomb, van der Waals or superexchange interactions with neighboring molecules in the crystal take place. Thus, the near-spherical symmetry of a molecule vibrating in solution is reduced to lower symmetry vibrations in an ordered crystal with an appropriate degeneracy decrease and splitting or broadening of the Raman lines. Another possibility is to investigate the change in the polarization characteristics of the Raman lines of the molecular vibrations in the crystal. It is well known that in anisotropic ensembles of molecules, such as single crystals, the Raman polarizations can yield information on the orientations of the molecules or their subgroups. By comparing protein-

ISSN 0907-4449

model coordinates available from the Brookhaven Protein Data Bank (PDB) with the polarized Raman spectra for a particular protein crystal, it is possible in principle to estimate the values of the components of the Raman tensor for a specific normal mode of vibration of the corresponding structural unit, and then to acquire information about the orientation of those units with respect to the crystallographic axes of the host crystal. This latter approach is explored in the present study.

2. Materials and methods

Tetragonal lysozyme crystals grown by two different methods were investigated. In the first method a 40 mg ml^{-1} solution of hen egg-white lysozyme (Calbiochem) was prepared by dissolving the protein in 1 ml of 50 m*M* acetate buffer (pH 4.6). A 3.5%(*w*/*v*) solution of NaCl was prepared by dissolving the salt in 1 ml of 50 m*M* acetate buffer (pH 4.6). Each solution was filtered through separate 0.22 µm Acrodisc filters. Growth solutions were prepared by mixing equal volumes (10 µl) of each solution on silanized glass cover slips, which were immediately placed into the apparatus used to grow the crystals. Crystals of lysozyme were grown using a dynamically controlled vapor-diffusion system which allows control of crystal nucleation and growth rates *via* the evaporation of water from the growth solutions. Crystals were grown at different evaporation rates in order to obtain crystals of varying quality. The crystals were mounted using silanized glass capillaries (Charles Supper Co.) of appropriate size to hold the desired crystals.

In the second method, lysozyme purchased from Seikagaku was dissolved in 50 m*M* acetate buffer and filtered to yield a 110 mg ml^{-1} stock solution. This solution was mixed in equal volume with a 5%(*w*/*w*) NaCl stock solution made from the same 50 m*M* buffer. 100 µl of the final preparation was injected in each of a set of thoroughly cleaned 200 µl micropipettes, which were then placed in an incubator at 274 K until small crystallites (about 10 µm) were visible on the walls. This occurred after about 24 h. The pipettes were then removed and each was kept at a different temperature to yield different supersaturations and, therefore, growth rates. The growth was documented by photographing the crystals at regular intervals.

The TLSCs were dried by exposure of the crystals to ambient atmosphere (293 K and 50% relative humidity). After this procedure, some crystals immediately cracked into smaller fragments, but a few did not lose their shape at all, only a few cracks appearing inside them. This latter case was usually observed for the better quality crystals. For Raman studies, we selected a crack-free part of the dehydrated crystal. It is necessary to mention that the present work is mostly devoted to the investigation of 'wet' crystals (those maintained at 100% relative humidity). 'Dry' crystals were studied to obtain supplementary information relative to the 'wet' crystal data.

In order to measure the Raman spectra, we have developed an experimental spectroscopic installation based on the high-throughput f/4 spectrograph, SpectraPro-150 (Acton Research Corporation) and a thermoelectrically cooled 256 × 1024 CCD camera from Princeton Instruments. As an excitation source we used a TEM_{00} linearly polarized He–Ne laser (λ = 632.8 nm). A 1200 grooves mm^{-1} grating, optimized for the red spectral region (blazed at 750 nm), was installed in the spectrograph. A schematic drawing of the experimental arrangement is shown in Fig. 1. The laser power at the sample did not exceed 3 mW. Low-power excitation allowed us to prevent thermal damage to the sample, making the setup completely non-invasive. A backscattering scheme was used to collect the Raman signal. In order to prevent the excitation wavelength from entering the spectrograph we used a holographic supernotch filter (Kaiser Optical Systems) with an optical density of > 6 at 632.8 nm. The spectral bandwidth of the supernotch filter in the Stokes region was about 100 cm^{-1}. The spectrograph and CCD detector were controlled by a Pentium-based personal computer, which was also used to collect and analyze the experimental data (*WinSpec v1.3* software).

For measuring polarized Raman spectra, two polarizers were installed into the setup. A polarization rotator was inserted into the laser beam in order to change the direction of the electric vector of the laser radiation with respect to the sample crystallographic axes. An analyzer was mounted in front of the entrance slit of the spectrograph and selected the polarization of scattered radiation to be measured. For each crystal we obtained the spectra in different polarization geometries: *ZZ*, *ZY*, *YZ* and *YY*, as shown in Fig. 2. Because of the natural shape of the tetragonal lysozyme crystal, we transformed the crystal frame of reference (see Fig. 2) by rotation about the *Z* axis through an angle of 45°. Such a transformation is reasonable for a uniaxial crystal and will be taken into account below.

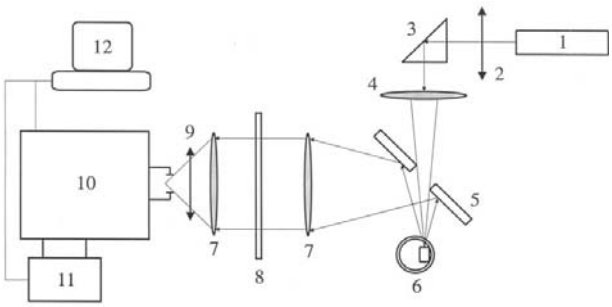

Fig. 1. Experimental setup. 1, He–Ne laser; 2, polarizer I (polarization rotator); 3, 90° prism; 4, focusing lens; 5, 45° mirror; 6, sample compartment (crystal mounted in the capillary); 7, focusing objective; 8, holographic supernotch filter; 9, polarizer II (analyzer); 10, spectrograph; 11, CCD camera; 12, personal computer.

In order to obtain pure polarized spectra, we had to remove the extrinsic depolarization caused by random multiple reflections of the excitation laser beam (and scattered radiation) inside the crystal and the capillary. In our experiments, the geometrical shape of the laser beam in the region of the interaction with the capillary can be imagined as a cylinder of 20–30 μm diameter and ~3 mm length (a 500 mm focusing lens was utilized), therefore, the focal-spot diameter was much less than the diameters of the capillaries used (1–3 mm). A collimated laser beam incident upon an empty capillary passes through four interfaces. At each interface reflection and refraction effects occur which, according to Fresnel's law, can modify the polarization parameters of the laser beam. Moreover, under some conditions (*i.e.* at some specific angles of incidence), these effects can produce multiple reflections inside the capillary cavity and wall owing to total internal reflection. Simple calculations based on the geometry show that when using a round capillary as an optical cell, the following capillary parameters are important: r/R (where r and R are the internal and external radii, respectively), the refractive index n of the capillary material and n^*/n (where n^* is the refractive index of the medium inside the capillary, which in this case is either the mother liquor or its saturated vapor). There are two ways to minimize the influence of multiple reflections: either by using capillaries with r/R as close to 1 as possible, *i.e.* with small wall thickness compared to radius, or by filling the capillary with a liquid having a refraction index close to that of the capillary material. In the present experiments we utilized glass ($n \simeq 1.5$) capillaries of two types which fulfilled the above requirements: (i) $R = 3.0$ mm, $d = 0.03$ mm (very fragile), $r/R = 0.98$. The internal media was the saturated vapor of the mother liquor ($n^* \simeq 1.0$); (ii) $R = 2.25$ mm, $d = 0.05$ mm, $r/R = 0.96$. The internal media was the mother liquor ($n^* \simeq 1.33$).

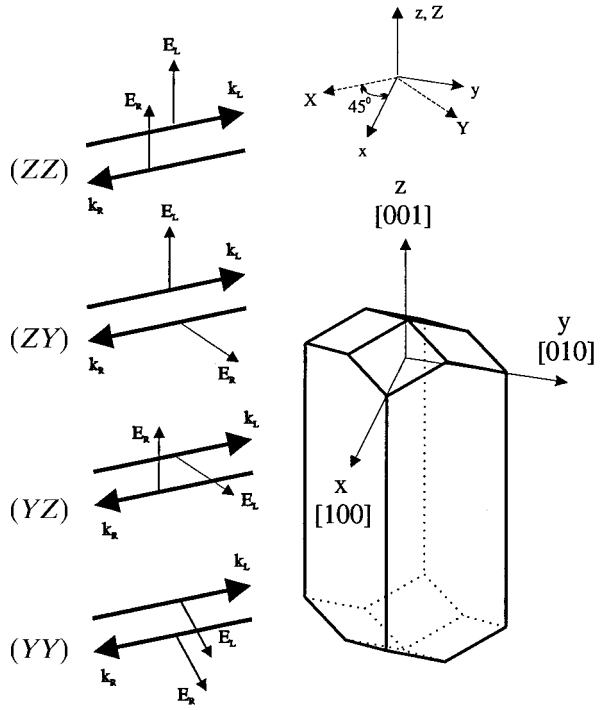

Fig. 2. Polarization geometries utilized in the experiments. E_L, polarization of laser light; E_R, polarization of the analyzed Raman light.

Multiple reflections within the protein crystal itself were eliminated simply by selecting crystals with dimensions much larger than the laser focal spot and with appropriate orientation within a capillary. Since a TLSC is transparent to visible light, the laser beam is easily transmitted through the whole thickness of the crystal. The undistorted profile of the laser beam exiting the capillary served as a good indicator for the absence of multiple reflections. We also explored another reason for the absence of extrinsic depolarization, namely, the practically complete suppression of Raman lines due to totally symmetric vibrations (mainly S—S, Trp, Tyr and Phe) measured in the ZY or YZ geometries (crossed polarizations of incident and scattered radiations) compared with the ZZ or YY geometries (parallel polarizations of the incident and scattered radiations).

Depolarization caused by the spectrograph and optical elements was estimated by comparing the relative intensities of the spectra taken in the ZY and YZ geometries. This is based on the fact that the Raman tensor for off-resonance scattering is symmetric ($\mathbf{a}_{ij} = \mathbf{a}_{ji}$) and, therefore, the intensities of the corresponding Raman lines in the above spectra must be equal.

Wet crystals were examined by X-ray diffraction to assess their relative quality. The diffraction resolution and the intensity of reflections from each crystal was measured using a Rigaku RU300 X-ray generator, a graphite monochromator and a Siemens X100A multiwire area detector. 50 frames of data were collected for each crystal and the data were processed using *Xengen v1.3*. In order to avoid degradation of lysozyme crystals due to X-ray exposure, the Raman measurements for each crystal were performed first. *RasMol v2.6* software was used to view the lysozyme three-dimensional structure. The atomic coordinates for tetragonal lysozyme crystals archived in the PDB were used in numerical simulations, which were performed with the help of the *SigmaPlot* Transform and Curve Fitting feature (*SigmaPlot v3.03*, Jandel Scientific). Deconvolution of the complex Raman bands was accomplished by means of *PeakFit v4.02* software (Jandel Scientific).

3. Experimental results

We were able to obtain good polarized Raman spectra for five wet and two dry tetragonal lysozyme single crystals. The relative quality of each wet crystal was

estimated *via* inspection under a microscope in addition to the X-ray diffraction analysis. Typical polarized Raman spectra of a wet TLSC taken in the *ZZ*, *YY* and *ZY* geometries are shown in Fig. 3. From Fig. 3 the following conclusions can be drawn. (i) The Raman lines at 507, 528, 543, 759, 834, 855, 875, 898, 930, 1004, 1012, 1103, 1196, 1208, 1302 and 1361 cm^{-1} (indicated in Fig. 3*a* by thin arrows) are caused by totally symmetric vibrations since they have a depolarization ratio, $\rho = I_\perp/I_\parallel$ close to zero ($I_\perp$ and $I_\parallel$ are the intensities of the Raman line measured with crossed and parallel polarizers, respectively). The assignment of the lines is mainly ascribable to totally symmetric vibrations of several components of the protein: the S—S disulfide bridges (at 507 and 528 cm^{-1}), the Trp side chains (543, 759, 875, 1012 and 1361 cm^{-1}), the Tyr side chains (834, 855 and 1208 cm^{-1}) and the Phe side-chain residues (1004 and 1196 cm^{-1}). (ii) The Raman bands at 1257, 1333, 1446 and 1621 cm^{-1} (indicated in Fig. 3*c* by bold arrows) are caused by asymmetric vibrations since they have a depolarization ratio close to 1 [or, more exactly, to 0.75 (Carey, 1982)]. The band at 1446 cm^{-1}, caused by deformational vibrations of CH_2 and CH_3 groups, has a high intensity and is well separated in the lysozyme Raman spectrum. Therefore, this band was used for normalization of the Raman spectra measured in the different polarization geometries. (iii) The Raman bands at 1554 cm^{-1} (Trp) and 1658 cm^{-1} (Amide I) are partially depolarized (indicated in Fig. 3*c* by unfilled arrows).

The above conclusions were reached on the basis of comparison between the Raman spectra taken in the *ZY* (crossed polarization of the incident and scattered light) and the *ZZ* or *YY* (parallel polarization of the incident and scattered light) geometries. Information can also be acquired by comparing spectra measured in the *ZZ* and *YY* geometries when the incident and scattered radiations have electric vectors which are parallel to each other, but parallel and perpendicular to the crystal *Z* axis, respectively. It can be seen from Figs. 3(*a*) and 3(*b*) that some lines have different relative intensities in the *ZZ* and *YY* spectra. This effect is the most pronounced for the 507 and 528 cm^{-1} Raman lines, which originate from the totally symmetric stretch vibration of the disulfide S—S bridges. These vibrational modes will be concentrated upon in the following discussion.

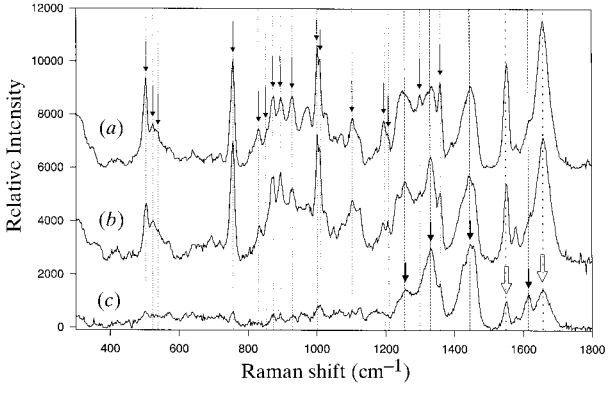

Fig. 3. Polarized Raman spectra of the lower-quality TLSC: (*a*), (*b*) and (*c*) correspond to the *ZZ*, *YY* and *YZ* polarization geometries, respectively. Strongly polarized Raman lines (totally symmetric vibrations) are indicated by thin arrows, strongly depolarized Raman lines (asymmetric vibrations) by bold arrows and partially depolarized Raman lines by unfilled arrows. Spectrum *c* has been normalized by a factor of 1/0.75 so that there is equal peak intensity of the Raman band at 1446 cm^{-1}.

It is well known from Raman studies of compounds containing disulfide bridges that a totally symmetric stretch vibration of an S—S bridge yields a Raman line located at a frequency of around 500 cm^{-1} (Sugeta *et al.*, 1972; van Wart *et al.*, 1973). Within a protein structure, such a vibration can be considered as a linear vibrational motion of the diatomic S—S groups, as the S atoms are heavy and electron-rich compared to C. The presence of C atoms in the disulfide bridge $C_\alpha—C_\beta—S—S—C_\beta'—C_\alpha'$ will perturb the above vibration. This perturbation depends on the conformation of the C atoms in the disulfide bridge (Sugeta *et al.*, 1972; van Wart *et al.*, 1973). It has been determined that the vibration at 510 ± 5 cm^{-1} is due to the *gauche-gauche-gauche* (ggg) conformation. The *gauche-gauche-trans* (ggt) rotamer is responsible for the Raman line at 525 ± 5 cm^{-1} and the *trans-gauche-trans* (tgt) rotamer for the line at 540 ± 5 cm^{-1} (van Wart *et al.*, 1973). According to the X-ray structural analysis of lysozyme (Blake *et al.*, 1967), three of the four disulfide bridges (Cys6—Cys127, Cys30—Cys115 and Cys64—Cys80) have a ggg conformation whilst the remaining one (Cys76—Cys94) has a ggt conformation. Therefore, the strong line at 507 cm^{-1} (Fig. 3) in the Raman spectrum of TLSC may be assigned to the three ggg disulfide bridges and the line with lower intensity at 528 cm^{-1} can be assigned to the ggt disulfide bridge. The relatively weak line at 543 cm^{-1} is probably due to tryptophan (Lord & Yu, 1970).

In Figs. 4(*a*)–4(*c*), the *ZZ* and *YY* Raman spectra in the region 400–800 cm^{-1} for three different TLSCs are presented. A dehydrated crystal is included for purposes of comparison. Before further consideration it is convenient to introduce the following designations. I_{ggg}^{ZZ} and I_{ggg}^{YY} represent the intensities of the ggg Raman line in the *ZZ* and *YY* spectra, respectively; I_{ggt}^{ZZ} and I_{ggg}^{YY} represent the intensities of the ggt Raman line in the *ZZ* and *YY* spectrum respectively;

$$\rho_0^{ZZ} = I_{ggg}^{ZZ}/I_{ggt}^{ZZ}, \quad \rho_0^{YY} = I_{ggg}^{YY}/I_{ggt}^{YY},$$
$$\rho_{ggg} = I_{ggg}^{ZZ}/I_{ggg}^{YY}, \quad \rho_{ggt} = I_{ggt}^{ZZ}/I_{ggt}^{YY}.$$

For all crystals studied, the following general regularities were observed in the polarized Raman spectra (see Figs. 4*a*–4*c*): $I_{ggt}^{ZZ} \simeq I_{ggt}^{YY}$, hence $\rho_{ggt} \simeq 1$; $I_{ggg}^{ZZ} > I_{ggg}^{YY}$, hence $\rho_{ggg} > 1$ and $\rho_0^{ZZ} > \rho_0^{YY}$.

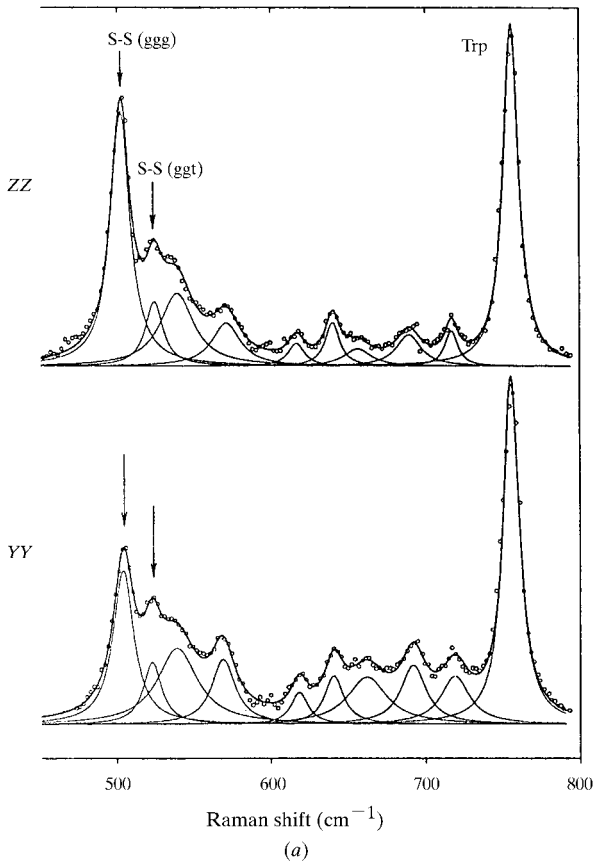

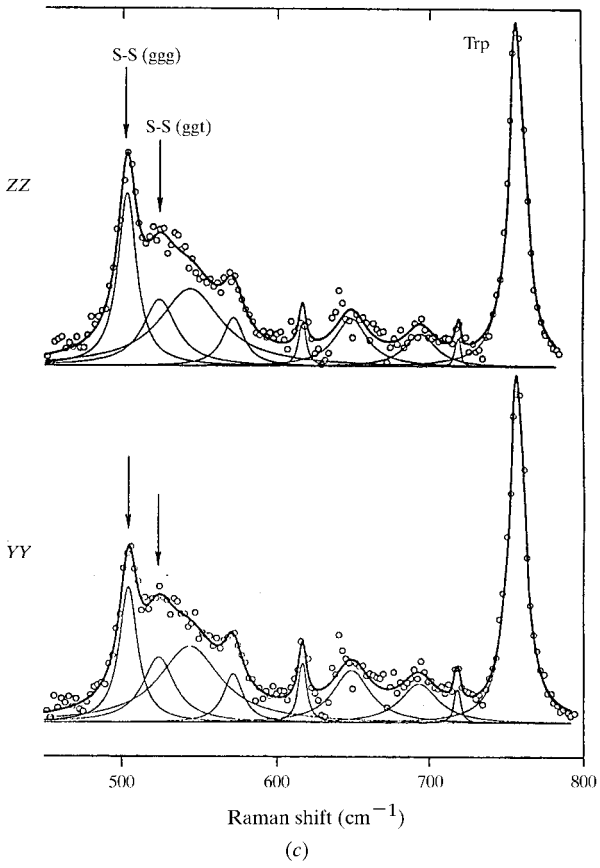

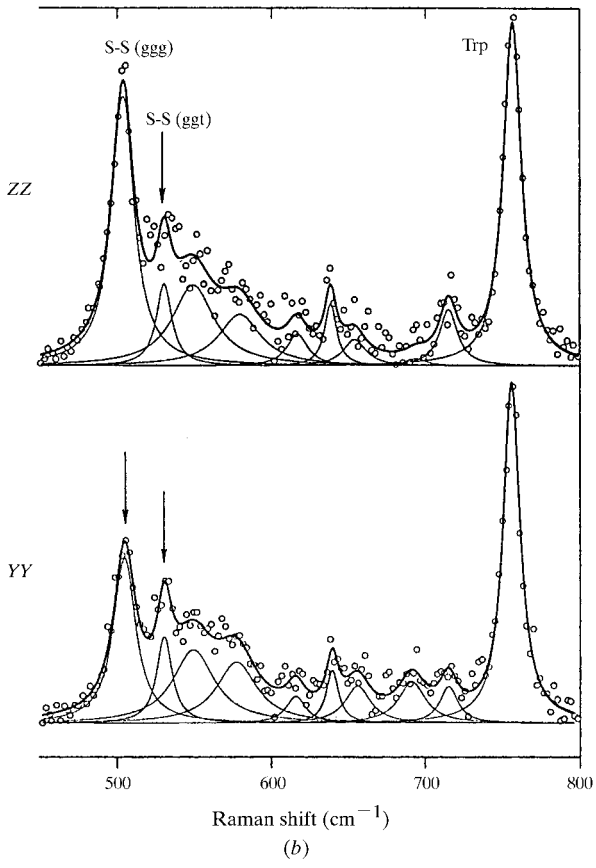

Fig. 4. Fragments of the polarized Raman spectra of (*a*) the lower quality TLSC, (*b*) higher quality TLSC and (*c*) dried TLSC in the spectral region 400–800 cm^{-1}.

Table 1. *The ρ_{ggg}, ρ_0^{ZZ} and ρ_0^{YY} values for different tetragonal lysozyme single crystals*

Sample	ρ_{ggg}	ρ_0^{ZZ}	ρ_0^{YY}
Crystal 1 (lower quality)	1.53	4.26	2.79
Crystal 2 (higher quality)	1.68	4.54	2.68
Simulation for PDB code 193L	1.46	4.56	3.13
Dried crystal	1.17	1.49	1.20

For wet crystals the range of ρ_{ggg} values was 1.50–1.68, whereas crystals of better quality had higher ρ_{ggg} values. The measured values of ρ_{ggg}, ρ_0^{ZZ} and ρ_0^{YY} for three different crystals are presented in Table 1.

The Raman spectra in the high-frequency region (2600–3800 cm^{-1}) were also measured for each crystal. In this frequency range the most prominent vibrational bands (including the totally symmetric stretch vibrations) of the C—H, N—H, and O—H groups are usually present (Tu, 1982). In Fig. 5, the Raman spectra of three different TLSCs, *i.e.* dried (Fig. 5*a*), lower quality (Fig. 5*b*) and higher quality (Fig. 5*c*) are presented together with that for a lysozyme solution (Fig. 5*d*). No significant differences were observed in the Raman spectra of the three crystals measured in the *ZZ* and *YY* polarization geometries. This is due to the fact that the TLSCs consist of a large number of randomly oriented C—H, N—H and O—H bonds. The C—H and N—H bonds are mostly within the protein molecule whilst the O—H bonds are mostly within the crystal lattice and belong to water groups. Fig. 5 shows that the integrated intensity of the O—H Raman band is noticeably higher for the higher quality TLSC than the crystal of lower quality.

4. Interpretation of the experimental results

The interpretation of the regularities in the polarized Raman spectra of the different quality TLSCs has been performed using three-dimensional structural data available from the PDB for several TLSCs. We judge the quality of those TLSCs mainly by the X-ray diffraction resolution limits and from comments in the corresponding references.

First, it is necessary to estimate the components of the Raman tensor for the totally symmetric stretch vibration of the disulfide bridges. As stated earlier, as a first approximation the vibration of such units can be considered as a linear vibration of the diatomic S—S units. We examined the general case when all diagonal components of the Raman tensor $\mathbf{R}_{ij}$ $(i, j = x, y, z)$ for a totally symmetric stretch vibration of the homonuclear diatomic unit are not equal to zero (in the principal *xyz* coordinate system, where the bond direction is parallel to the *z* axis). This can be represented by

$$\mathbf{R}_{ij} = \begin{vmatrix} r_{xx} & 0 & 0 \\ 0 & r_{yy} & 0 \\ 0 & 0 & r_{zz} \end{vmatrix},$$

where $r_{xx} = d\alpha_{xx}/dz$, $r_{yy} = d\alpha_{yy}/dz$, $r_{zz} = d\alpha_{zz}/dz$, r_{xx}, r_{yy}, $r_{zz} \neq 0$ and α_{ij} is the polarizability tensor. Because of the $D_{\infty h}$ symmetry of the homonuclear diatomic unit $r_{xx} = r_{yy}$ and the following designations can be made: $r_{xx} = r_{yy} = a$, $r_{zz} = b$ and $a, b \neq 0$. For each vibrational band, the Raman intensity measured in a polarization geometry *IS* (where *I* and *S* are the polarizations of the incident and scattered light, respectively) can be written as

$$I^{IS} = A\left(\sum_{\alpha,\beta=x,y,z} e_I^{\alpha} r_{\alpha\beta} e_S^{\beta}\right)^2,$$

where *A* is a constant and e_I^{α} and e_S^{β} are the components of the unit electric vectors of the incident (*I*) and scattered (*S*) photons along the principal axes α and β of the Raman tensor (see, for example, Wilkinson, 1973). If θ and φ are the polar angles, which determine the spatial orientation of the diatomic unit with respect to a fixed

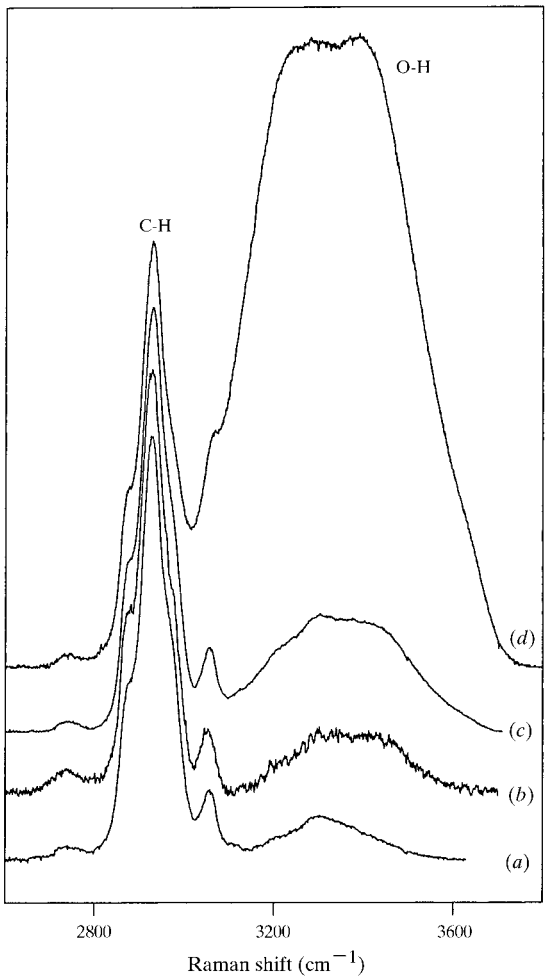

Fig. 5. Raman spectra of different lysozyme crystals and lysozyme solution in the high-frequency region. (*a*), Dried crystal; (*b*), lower quality crystal; (*c*), higher quality crystal; (*d*), lysozyme solution (150 mg ml^{-1}).

XYZ coordinate system corresponding to the crystallographic axes of tetragonal lysozyme, then the intensity of the Raman line due to a totally symmetric stretch vibration measured in the *ZZ*, *YY* and *XX* geometries can then be written as

$$I^{ZZ} = A(a\sin^2\theta + b\cos^2\theta)^2 \quad (1a)$$

$$I^{YY} = A(a\cos^2\theta\sin^2\varphi + b\sin^2\theta\sin^2\varphi + a\cos^2\varphi)^2 \quad (1b)$$

$$I^{XX} = A(a\cos^2\theta\cos^2\varphi + b\sin^2\theta\cos^2\varphi + a\sin^2\varphi)^2. \quad (1c)$$

The first-order Raman spectrum of a single crystal is a reflection of the vibrational motions of a discrete unit cell. For tetragonal lysozyme, the unit cell has $P4_32_12$ space-group symmetry and contains eight molecules. The spatial arrangement of the lysozyme molecules within the tetragonal unit cell is clearly shown in the recent paper by Nadarajah & Pusey (1996), in which eight molecules with a unique orientation can be separated into two groups denoted by (*M*, *A*, *B*, *C*) and (*D*, *E*, *F*, *G*). Let us call the first group I and the second group II. Within groups I and II, the molecules are related *via* the 4_3 screw-axis symmetry. Additionally, each molecule from group I is related by twofold symmetry to the corresponding molecule from group II (and *vice versa*). As a result, these two molecules have an opposite orientation along the 4_3 axis.

Let us consider a single S—S bond in each molecule. Since I^{ZZ} does not depend on φ, it will have the same value for both groups,

$$I_{\rm I}^{ZZ} = I_{\rm II}^{ZZ} = I^{ZZ} = 4A(a\sin^2\theta + b\cos^2\theta)^2. \quad (2a)$$

Because of the dependence of I^{YY} (and I^{XX}) on the angle φ, the quantities I^{YY} (and I^{XX}) will differ between group I and group II. For group I

$$I_{\rm I}^{YY} = 2A(B\sin^2\varphi^{\rm I} + a\cos^2\varphi^{\rm I})^2 + 2A(B\cos^2\varphi^{\rm I} + a\sin^2\varphi^{\rm I})^2, \quad (2b)$$

and for group II

$$I_{\rm II}^{YY} = 2A(B\sin^2\varphi^{\rm II} + a\cos^2\varphi^{\rm II})^2 + 2A(B\cos^2\varphi^{\rm II} + a\sin^2\varphi^{\rm II})^2, \quad (2c)$$

where $\varphi^{\rm I}$ is the φ angle for the first molecule of group I, $\varphi^{\rm II}$ is the φ angle for the first molecule of group II and $B = a\cos^2\theta + b\sin^2\theta$. Values of φ for the other molecules in the group, φ_n, are related to $\varphi^{\rm I}$ and $\varphi^{\rm II}$ by

$$\varphi_n^{\rm I} = \varphi^{\rm I} + (n-1)\pi/2$$
$$\varphi_n^{\rm II} = \varphi^{\rm II} + (n-1)\pi/2,\ \ \varphi^{\rm II} = 90^\circ - \varphi_n^{\rm I}.$$

B is the same for both groups since $\theta^{\rm II} = 180^\circ - \theta^{\rm I}$.

Let the orientation of each S—S bridge of a lysozyme molecule be determined by the θ_i and φ_i polar angles. If it is assumed that the S—S units vibrate independently within the protein molecule (Clarage *et al.*, 1992), then for the ggt (i = 0) and ggg (i = 1, 2, 3) Raman line intensities the following relationships can be derived.

$$\rho_0^{ZZ} = I_{\rm ggg}^{ZZ}/I_{\rm ggt}^{ZZ} = \Big[\sum_{i=1}^{3}(I^{ZZ})_i\Big]/(I^{ZZ})_0 \quad (3a)$$

$$\rho_0^{YY} = I_{\rm ggg}^{YY}/I_{\rm ggt}^{YY} = \Big[\sum_{i=1}^{3}(I_{\rm I}^{YY} + I_{\rm II}^{YY})_i\Big]/(I_{\rm I}^{YY} + I_{\rm II}^{YY})_0 \quad (3b)$$

$$\rho_{\rm ggg} = I_{\rm ggg}^{ZZ}/I_{\rm ggg}^{YY} = \Big[2\sum_{i=1}^{3}(I^{ZZ})_i\Big]/\Big[\sum_{i=1}^{3}(I_{\rm I}^{YY} + I_{\rm II}^{YY})_i\Big] \quad (3c)$$

$$\rho_{\rm ggt} = I_{\rm ggt}^{ZZ}/I_{\rm ggt}^{YY} = [2(I^{ZZ})_0]/(I_{\rm I}^{YY} + I_{\rm II}^{YY})_0. \quad (3d)$$

As mentioned above, the numerical values for all these quantities can be obtained from the experimental Raman spectra.

Table 2 lists the characteristics (θ_i, φ_i and *B* factors) of the four disulfide bonds in one particular tetragonal lysozyme structure (PDB code 193L, Vaney *et al.*, 1996) that are, with the exception of the *B* factors, derived from the atomic coordinates. The *B* factor for each disulfide bond has been obtained by taking the arithmetic mean of the *B* factors of the constituent S atoms.

The structural data in Table 2 have been obtained from a crystal which diffracted to a maximum resolution of ~1.33 Å (Vaney *et al.*, 1996). These data we therefore refer to as being derived from a high-quality tetragonal lysozyme crystal.

Let the crystal be rotated around the *Z* axis by an angle Φ. All the quantities ($\varphi_n^{\rm I,II}$) in the expressions for $I_{\rm I}^{YY}$ and $I_{\rm II}^{YY}$ must then be replaced by ($\varphi_n^{\rm I,II} + \Phi$). Simple analysis of (2*b*) and (2*c*) shows that for $\Phi = \pi l/4$, (l = 0, 1, 2, ...) $I_{\rm I}^{YY} = I_{\rm II}^{YY}$. Our experimental data is given for $\Phi = 45^\circ$. For this reason, in the further considerations below, we will often take into account only the four molecules of group I when this does not affect the final results.

Let us compare the quantities ρ_0^{ZZ}, ρ_0^{YY}, $\rho_{\rm ggg}$ and $\rho_{\rm ggt}$, which are calculated using the data from Table 2 and (3*a*)–(3*d*), with the experimental quantities determined from the Raman spectra (Table 1).

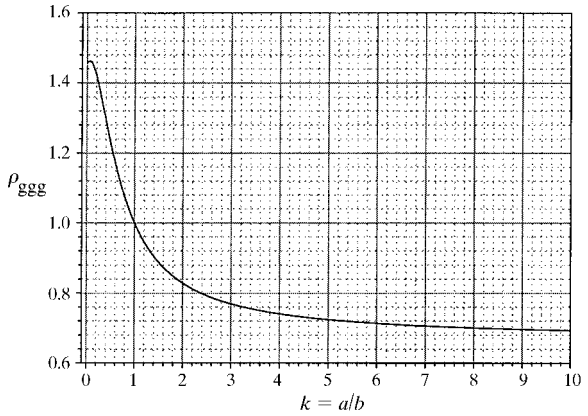

Fig. 6. Plot of $\rho_{\rm ggg}$ as a function of $k = a/b$ calculated with equation (3*c*) for the three ggg disulfide bonds of the lysozyme molecule within a close-to-perfect tetragonal lattice (PDB code 193L).

Table 2. *The characteristics of the disulfide bonds for tetragonal lysozyme (PDB code 193L)*

S—S bond	Conformation	θ_i (°)	φ_i (°)	$\langle B \rangle$ (Å^2)
76–94	ggt	$\theta_0 = 23.7$	$\varphi_0 = -158.1$	14.30
64–80	ggg	$\theta_1 = 87.2$	$\varphi_1 = -39.5$	10.67
30–115	ggg	$\theta_2 = 25.1$	$\varphi_2 = 10.75$	11.08
6–127	ggg	$\theta_3 = 45.6$	$\varphi_3 = 129.4$	18.12

The plot of the calculated values of ρ_{ggg} as a function of $k = a/b$ is shown in Fig. 6. It can be seen from Fig. 6 that for the best fit to the experimental data, the quantity k must be close to zero. In this case, from (3*c*) we obtain ρ_{ggg} (0) = 1.46. On the other hand, the experimental value for ρ_{ggg} has a range 1.50–1.68. Thus, we have to assume that $b \gg a$ (effectively, $a = 0$, $b \neq 0$).

Figs. 7 and 8 show the values of ρ_{ggt}, ρ_0^{ZZ} and ρ_0^{YY} as a function of a/b, as simulated with (3*a*)–(3*d*). These plots contradict the experimental data, namely those which suggest that $\rho_{ggt} \simeq 1$ and $\rho_0^{ZZ} > \rho_0^{YY}$. From Fig. 7 one can conclude that $\rho_{ggt} = 1$ only when $k = 1$ and from Fig. 8 that $\rho_0^{ZZ} > \rho_0^{YY}$ only when $k > 1$. These conclusions do not make sense. The reasonable way to resolve this contradiction is to assume full orientational disorder of the ggt bonds of the lysozyme within the tetragonal lattice. The remoteness from intermolecular contacts and increased value of the *B* factor for the ggt bond of the lysozyme molecule support this assumption.

Thus, for a ggt disulfide bond randomly oriented within the crystal, as assumed above, the appropriate expressions for the Raman intensities can be written as follows (for the molecules of group I):

$$I_{ZZ} = I_{YY} = I_{XX} \simeq 4c^2,$$

where c is a constant. For this case, we immediately obtain $\rho_{ggt} = 1$. The corresponding plots of ρ_0^{ZZ} and ρ_0^{YY} as a function of $m = (b/c)^2$ are presented in Fig. 9. Here, it is worth mentioning that the above assumption gives the correct relationship $\rho_0^{ZZ} > \rho_0^{YY}$, which correlates with the experimental data. For an equiprobable distribution of a ggt S—S bond orientation within 4π, the averaging procedure gives

$$\langle I_{ZZ} \rangle = \langle I_{YY} \rangle = \langle I_{XX} \rangle = \frac{\int_0^{2\pi} d\varphi \int_0^{\pi} b^2 \cos^4\theta \sin\theta d\theta}{\int_0^{2\pi} d\varphi \int_0^{\pi} \sin\theta d\theta} = \frac{b^2}{5}.$$

Hence, $m = 5$. For this value of m we obtain, from Fig. 9, $\rho_0^{ZZ} = 4.56$ and $\rho_0^{YY} = 3.13$. These values are close to the experimental values for a TLSC of high quality, somewhat higher for a TLSC of lower quality and much higher for a dried TLSC (see Table 1). This tendency can be explained as follows. The model we are exploring assumes that all three ggg S—S bridges have the same vibrational frequency. Hence, the intensity of the resulting ggg line is simply a sum of the intensities of three separate disulfide bonds (isofrequency summation). However, it appears that this is not completely true for tetragonal lysozyme. After the deconvolution procedure (*PeakFit v4.02* by Jandel Scientific) of the polarized Raman spectra of the disulfide bonds in TLSC, a small but noticeable frequency shift ($\Delta \simeq 1$ cm^{-1}) between the centers of the ggg Raman lines was measured in the *ZZ* and *YY* polarization geometries. The line measured in the *ZZ* geometry has a lower frequency (red shift) than the line measured in the *YY* polarization configuration. The Δ values are 0.9 cm^{-1} for a high-quality crystal, 1.4 cm^{-1} for a lower quality TLSC and 1.7 cm^{-1} for a dried crystal. As derived from the PDB data (PDB code 193L), there is a small variation in the bond lengths between the three ggg disulfide bridges of lysozyme in the tetragonal lattice; the lengths are 2.021, 2.029 and 2.031 Å for the 6–127, 64–80 and 30–115 S—S bridges, respectively. This is probably caused by some conformational difference between the S—S bridges (the positions of the C atoms in the disulfide bridge $C_\alpha—C_\beta—S—S—C_\beta'—C_\alpha'$ have to be taken into account). The 30–115 ggg S—S bond makes the main

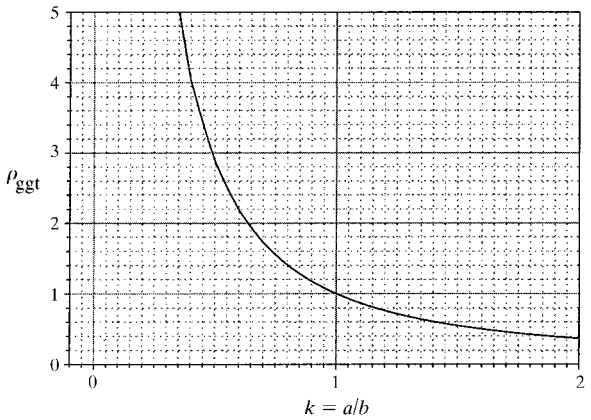

Fig. 7. Plot of ρ_{ggt} as a function of $k = a/b$ simulated with equation (3*d*) for the single ggt disulfide bond of the lysozyme molecule in the tetragonal lattice.

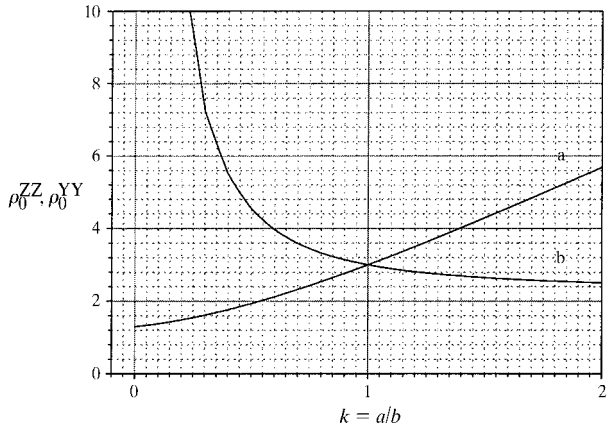

Fig. 8. Plots of ρ_0^{ZZ} (curve *a*) and ρ_0^{YY} (curve *b*) as a function of $k = a/b$ simulated according to equations (3*a*) and (3*b*) for a tetragonal lysozyme crystal.

contribution to the *ZZ* Raman spectrum, since the orientation of this bond is the closest of the three ggg bridges to the *Z* axis (see Table 2). On the other hand, the S—S bridge 30–115 possesses the longest bond length (2.031 Å) among the ggg bonds. This means that the force constant and the magnitude of the vibrational frequency for this bridge must be the least of the ggg bonds. This clearly explains the above-mentioned red shift of the ggg Raman line measured in the *ZZ* geometry compared with the *YY* polarization configuration. Taking into account the values of Δ, ρ_0^{ZZ} and ρ_0^{YY} obtained for different TLSCs, we can conclude that the conformational variation between the ggg bridges is lowest for a high-quality TLSC. Yu & Jo (1973) measured the depolarized spectra of lysozyme in three different states: a solution (35 mg ml^{-1}), a fine polycrystalline powder at 100% relative humidity and a lyophilized powder. ρ_0 values can be estimated from the depolarized spectra. ρ_0 has a maximum value for the solution, a minimum for the lyophilized powder and an intermediate value for the polycrystalline powder at full humidity. In accordance with the above interpretation, these variations of ρ_0 can be explained by conformational variations between the ggg bridges of the lysozyme in the solution, crystal and dehydrated states. All three ggg bridges of the undistorted protein molecules in solution have similar conformations. Conversely, in the lyophilized state, strong intermolecular interaction causes distortion of the protein mainly at the contact points, which in turn probably leads to variation in conformation between ggg S—S bridges. Thus, ρ_0 probably correlates with the extent of the perturbation of the protein molecules. The higher the value of ρ_0, the weaker the perturbation. Taking into account the lower extent of the conformational variation within the ggg disulfide bonds in high-quality TLSCs, we can conclude that the extent of perturbation of the protein molecules is lower in crystals of better quality. The comparison of

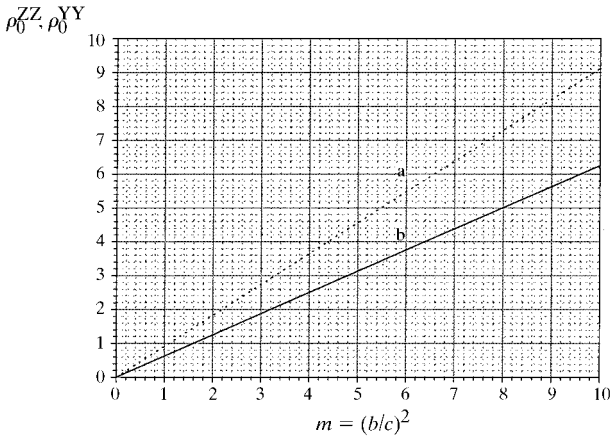

Fig. 9. ρ_0^{ZZ} (plot *a*) and ρ_0^{YY} (plot *b*) *versus* $m = (b/c)^2$ simulated for the case of the orientational disorder of ggt S—S bonds within a tetragonal lysozyme crystal.

corresponding values of ρ_0^{ZZ} and ρ_0^{YY} for wet and dehydrated crystals would not make sense here for the following reason. Kachalova *et al.* (1987) have measured the effect of dehydration on the X-ray diffraction of three crystal forms of lysozyme (including tetragonal) and have shown displacement of both the molecule as a whole and of the two domains of the lysozyme molecules relative to one another. Therefore, the orientation of S—S bonds should be quite different in a dried crystal compared with a wet crystal. Unfortunately, atomic coordinates are not available for dried lysozyme crystals.

It is known from X-ray diffraction data that the 64–80 (ggg) and 30–115 (ggg) disulfide bonds in lysozyme are buried in the structure and located close to the intermolecular contacts. On the other hand, the 6–127 (ggg) and the 76–94 (ggt) bonds are on the surface of the protein and distant from the intermolecular contacts. This probably explains the increased values of the averaged *B* factors for the 6–127 (ggg) and 76–94 (ggt) bridges in comparison to the 64–80 (ggg) and 30–115 (ggg) bridges (see Table 2). Taking these circumstances into consideration, it is reasonable to improve the proposed model by assuming full orientational disorder for the 6–127 (ggg) bonds as well as for the 76–94 (ggt) bonds. This would mean that the 6–127 (ggg) bonds have no preferential orientation within the crystal lattice. The main problem with this is that the value of $\rho_{ggg} = 1.19$ calculated for this case (PDB code 193L) is too low. Thus, the 6–127 S—S bonds having a definite average orientation within the crystal lattice better fits the experimental Raman data. Here, we probably need to take into account the anisotropy of the *B* factor due to its tensor character: $\mathbf{B}_{ij} = (\overline{u^2})_{ij}$ (i, j are the principal axes).

Let us summarize the main conclusions from the above interpretation. The model, which is consistent with both Raman and PDB data, can be described by the following attributes. (i) The totally symmetric stretch vibrations of the disulfide bonds can be regarded with good accuracy as diatomic units. The only non-zero component of the local Raman tensor (in the principal *xyz* coordinate system with the *z* axis parallel to the bond direction) is the *zz* component. (ii) In the tetragonal lysozyme crystal lattice, all three ggg disulfide bonds (64–80, 30–115 and 6–127) have a definite average orientation which can be derived from PDB data. The ggt bond (76–94) does not have a preferential orientation within the crystal lattice and therefore can be characterized by full orientational disorder.

The following information can be obtained from the polarized Raman spectra. (i) By measuring ρ_0^{ZZ} and ρ_0^{YY} (or ρ_0 from the depolarized spectra), as well as Δ (the red shift), one can judge the value of the vibrational-frequency variation between ggg bonds. It appears reasonable to ascribe this variation to the extent of the perturbation of the lysozyme molecules within the crystal lattice. As an indication of the lower conforma-

Table 3. *Crystallographic data available at the Protein Data Bank for tetragonal lysozyme crystals*

PDB code	Resolution (Å)	θ_1 (64–80) (°)	θ_2 (30–115) (°)	θ_3 (6–127) (°)	a (Å)	c (Å)	$\langle B \rangle$ (Å^2)	
193L	1.33	87.28	25.14	45.61	78.54	37.77	16.7	Earth-grown
194L	1.40	87.32	26.27	45.43	78.65	37.76	18.6	Space-grown
1LSF	1.70	88.43	22.68	41.45	76.996	37.132	22.11	95 K
1LSE	1.70	86.58	25.49	44.34	79.245	37.858	22.42	295 K
4LYM	2.10	86.90	25.50	41.08	78.4	37.6	22.57	Low-humidity form
3LYM	2.00	87.37	27.74	42.99	78.69	38.00	18.10	1000 at
2LYM	2.00	87.78	27.68	44.76	79.170	37.960	19.81	1 at
1HEL	1.70	85.25	26.75	45.24	79.1	37.9	18.79	Recombinant form
1LZB	1.50	86.12	25.95	43.87	78.72	38.46	15.35	+ Tri-*N*-acetylchitotriose

tional variation between ggg disulfide bonds, the higher values of ρ_0^{ZZ} (and ρ_0^{YY} to a lesser extent) and the lower values of Δ are reasonable. This situation, we believe, is characteristic for crystals of high quality. (ii) By measuring ρ_{ggg}, it is possible to judge the average orientation of the ggg disulfide bonds with respect to the 4_3 crystallographic axis.

Regarding the latter statement, we had good reason to presume that the average orientation of the ggg bonds should correlate with the orientation of the protein molecule itself, since the strong disulfide linkages in lysozyme are responsible for the high stability of its native conformation (Imoto *et al.*, 1972). In order to obtain additional evidence, we analyzed the PDB data available for nine tetragonal lysozyme crystals grown under different conditions (Table 3).

All the crystals listed in Table 3 are earth-grown (with the exception of 194L) and were studied at room temperature (except 1LSF), ambient pressure (except 3LYM) and 100% humidity (except 4LYM). In Fig. 10(*a*), the plot of θ_2 *versus* θ_1 for all crystals in Table 3 is shown. It can be seen from Fig. 10(*a*) that there is a definite correlation between θ_2 and θ_1 for all of the crystals except three: 194L, 2LYM and 3LYM (indicated in Fig. 10*a*). The dependence of θ_2 on θ_1 and *vice versa* means that there is a kinematic link between the 64–80 and 30–115 disulfide bridges. Since these bridges are distant from each other within the lysozyme molecule, this is a good reason to interpret the correlated change of θ_1 and θ_2 as being due to the rotation of the whole protein as a rigid body. This rotation can be attributed to the conditions of the crystal-growth process and/or to the ambient conditions (temperature, pressure and humidity). In Fig. 10(*b*), the plot of θ_3 *versus* θ_1 is presented. There is no obvious correlation between θ_3 and θ_1. This is consistent with the increased value of the B factor for 6–127 (ggg) S—S bonds.

Since the 30–115 and 64–80 bridges provide the main contribution I_{ggg}^{ZZ} and I_{ggg}^{YY}, respectively, they also define the real value of $\rho_{ggg} = I_{ggg}^{ZZ}/I_{ggg}^{YY}$. Therefore, the value of ρ_{ggg} obtained from polarized Raman spectra must correlate with the average orientation of the protein molecules with respect to the Z crystallographic axis. Taking into consideration the experimental values of ρ_{ggg} for crystals of different quality (Table 1), we can conclude that TLSCs of different quality are characterized by a difference in the average orientation of the constituent molecules with respect to the Z axis.

As previously mentioned, three points on the plot indicated in Fig. 10(*a*), corresponding to the crystals 194L, 2LYM and 3LYM, do not participate in the relationship between θ_1 and θ_2 observed for the other six crystals in Table 3. For the crystals 2LYM and 3LYM this may be due to systematic experimental error since they are investigated in the same paper. Crystal 194L is the only space-grown crystal listed in Table 3.

In order to evaluate the sensitivity of the Raman method described, three specific cases must be considered. The first two are related to the error in the crystal orientation with respect to the polarization of incident and scattered light. The third is associated with useful information regarding the average orientation of the proteins with respect to the Z axis, which can be determined from the Raman spectra.

In case 1, the crystal is rotated as a whole about the X axis by a small angle $\Delta\psi = \pm 5^\circ$. The dependence of ρ_{ggg} on $\Delta\psi$ illustrates the effect of the error in the alignment of the electric vectors of the excitation and scattered light with respect to the Z and Y crystallographic axes of the sample. Again, the four molecules which are related by 4_3 symmetry at $\Delta\psi = 0^\circ$ are considered. When $\Delta\psi \neq 0^\circ$, the 4_3 symmetry will be broken in the fixed-coordinate system. In this case, for each of the three ggg bonds, the following relationships can be derived, where i refers to the ggg bond number (i = 1–3) and n refers to the molecule number (n = 1–4),

$$\varphi_{in}(\Delta\psi) = \arctan\{M_{in} \sin[\psi_{in}^{(0)} + \Delta\psi]\} \qquad (4a)$$

$$\theta_{in}(\Delta\psi) = \arctan(\{\tan[\psi_{in}^{(0)} + \Delta\psi]\}/\sin\varphi_{in}, \qquad (4b)$$

where $\psi_{in}^{(0)}$ is the angle between the Z axis and the projection of the ggg bond onto the ZY plane when $\Delta\psi = 0^\circ$. M_{in} does not depend on $\Delta\psi$ for the transformation considered and can be calculated using the data from the PDB $\{M_{in} = [(\beta_{in}^2 + \gamma_{in}^2)/\alpha_{in}^2]^{1/2}$, where α, β and γ are the corresponding projections of the *in* disulfide bond along the X, Y and Z axes, respectively$\}$. Substituting φ and θ from (4*a*) and (4*b*) into (1*a*) and (1*b*) and

taking the sum over all ggg bonds of the four molecules in group I gives the final expression

$$\rho_{ggg}(\Delta\psi) = \frac{\sum_{i=1}^{3}\sum_{n=1}^{4} \cos^4 \theta_{in}}{\sum_{i=1}^{3}\sum_{n=1}^{4} \sin^4 \theta_{in} \sin^4 \varphi_{in}}. \qquad (5)$$

The plot of $\rho_{ggg}(\Delta\psi)$ as a function of $\Delta\psi$, calculated according to (5), is presented in Fig. 11 (curve *a*). The values of $\psi_{in}^{(0)}$ obtained from X-ray diffraction data (PDB code 193L) are listed in Table 4.

In case 2, the crystal is rotated as a whole about the Z axis by a small angle $\Delta\varphi = \pm 5^\circ$. The dependence of ρ_{ggg} on $\Delta\varphi$ shows the effect of the error in the alignment of the electric vectors of the excitation and scattered light with respect to the Y (or X) crystallographic axis of the sample. The 4_3 symmetry is preserved during such a transformation, in contrast to the previous case. Here one must take into account the molecules of both groups I and II, since they give equal contributions to I^{YY} only when $\Delta\varphi = 0$ (see above). The expressions (4*a*) and (4*b*) will now have the following forms,

$$\varphi_{in}(\Delta\varphi) = \arctan(M_{in} \sin \psi_{in}) \qquad (6a)$$

$$\theta_{in}(\Delta\varphi) = \arctan(\tan \psi_{in} / \sin \varphi_{in}), \qquad (6b)$$

where $\psi_{in} = \psi_{in}(\Delta\varphi)$ and $M_{in} = M_{in}(\Delta\varphi)$ at the transformation considered. Substituting φ and θ from (6*a*) and (6*b*) into (2*a*), (2*b*) and (2*c*), and finally into (3*c*), gives the resulting expression for ρ_{ggg} as a function of $\Delta\varphi$. The plot of $\rho_{ggg}(\Delta\varphi)$, simulated in accordance with the above procedure, is presented in Fig. 11 (curve *b*). In principle, an error of this kind can be significantly reduced by monitoring the direction of the laser-beam reflection from the front crystal face.

In case 3, the first molecule of group I ($n = 1$) is rotated about the X axis in exactly the same way as in case 1 ($\Delta\psi' = \pm 5^\circ$). Each of the remaining three molecules is rotated the same way as the first molecule but with respect to the Z axis. Again, the 4_3 symmetry is preserved during this transformation, in contrast to case 1. The dependence of ρ_{ggg} as a function of $\delta\psi'$ suggests the possibility of estimating the average orientational ordering of the protein molecules in the crystal lattice with the help of the polarized Raman spectra, provided that the orientation of the *ggg* S—S bridges correlates

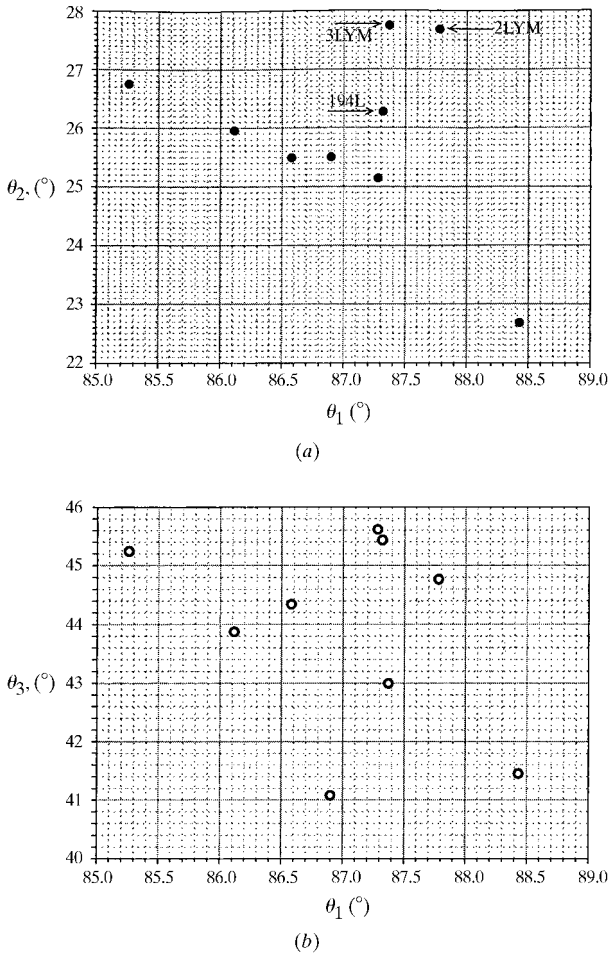

Fig. 10. (*a*) Plot of θ_2 and (*b*) plot of θ_3 *versus* θ_1 for nine tetragonal lysozyme crystals, X-ray diffraction data of which are available at the Protein Data Bank.

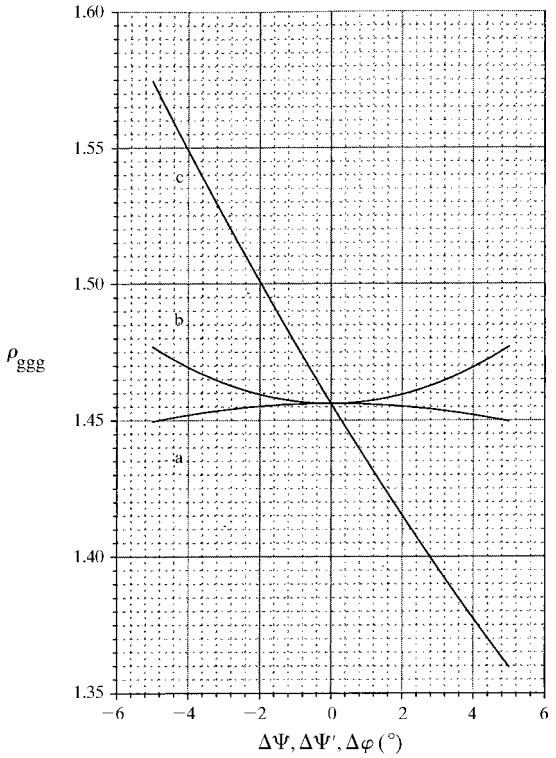

Fig. 11. Plots of $\rho_{ggg}(\Delta\psi)$ (curve *a*), $\rho_{ggg}(\Delta\varphi)$ (curve *b*) and $\rho_{ggg}(\Delta\psi')$ (curve *c*).

Table 4. *The values of* $\psi_{in}^{(0)}(^\circ)$ *for the three ggg S—S bonds in four lysozyme molecules related by* 4_3 *symmetry within a tetragonal lattice (PDB code 193L)*

ggg S—S bond	Molecule 1 (n = 1)	Molecule 2 (n = 2)	Molecule 3 (n = 3)	Molecule 4 (n = 4)
64–80 (i = 1)	−85.6	86.4	85.6	−86.4
30–115 (i = 2)	38.3	−33.0	−38.3	33.0
6–127 (i = 3)	5.0	24.75	−5.0	−24.75

with the orientation of the whole protein molecule, which is a reasonable assumption.

Taking into account the formulae (2*a*), (2*b*), (4*a*) and (4*b*), as well as the θ_{i1} and φ_{i1} data from Table 2 and the $\psi_{i1}^{(0)}$ data from Table 4, we can write the following expression (considering three ggg bonds i = 1–3 for the first molecule only),

$$\rho_{ggg}(\Delta\psi') = \frac{2\sum_{i=1}^{3}\cos^4\theta_{i1}}{\sum_{i=1}^{3}(\sin^4\varphi_{i1} + \cos^4\varphi_{i1})\sin^4\theta_{i1}}. \qquad (7)$$

The plot of $\rho_{ggg}(\Delta\psi')$ as a function of $\Delta\psi'$ calculated according to (7) is presented in Fig. 11 (curve *c*).

Fig. 11 shows that within the error of the alignment of the electric vectors of the laser and scattered radiations ($\Delta\psi_{err} \simeq \pm 1^\circ$) with respect to the crystal axes, the $\rho_{ggg}(\Delta\psi)$ value varies within $\pm 9 \times 10^{-3}$% (Fig. 11, curve *a*). Such a change in $\rho_{ggg}(\Delta\psi')$ would correspond to a variation in the extent of the average orientation of the protein molecules along the Z axis of the order of $\Delta\psi'_{ord} \simeq 45''$ (Fig. 11, curve *c*). This number is much lower than the real values of the variation of the average angles of protein orientation for different crystals, which can be of the order of 1°. This means that the main source of error in the experimental value of ρ_{ggg} is not the accuracy of the crystal orientation ($\pm 1^\circ$ in present work) but standard features of the Raman spectra such as the signal-to-noise ratio, the level of the background signal *etc.*, which can be considerably reduced by utilizing a modern Raman setup. Thus, the sensitivity of the method described is sufficient for registration of the change in the average orientational ordering of the lysozyme molecules within the tetragonal lattice.

For the Raman spectra in the high-frequency region 2600–3800 cm^{-1} (see Fig. 5), we took into account the fact that the Raman C—H and N—H bands are intrinsic to the protein and the O—H band is mostly intrinsic to the water molecules (both ordered and free). Therefore, it is possible to estimate roughly the relative water content of the crystal by calculating the ratio of the integrated intensities of the C—H and O—H Raman bands. The possible overlap of the O—H and N—H bands will not significantly affect this estimation, since the measured intensity ratio will correspond to the real intensity ratio I_{OH}/I_{CH} plus a constant value I_{NH}/I_{CH}. Since all the spectra shown in Fig. 5 are normalized to the peak intensity of the maximum at 2930 cm^{-1} (assignable to the totally symmetric stretch vibration of the CH_3 functional groups), the increasing integrated intensity of the O—H band in the sequence dried crystal → lower-quality crystal → higher quality crystal (Figs. 5*a*–5*c*) shows an increase in water content. The detailed analysis of the TLSC Raman spectra in the high-frequency region will be published elsewhere.

5. Conclusions

Generally accepted criteria for the quality of protein crystals associate one type of crystal imperfection with the presence of mosaic blocks (Helliwell, 1988). The measured rocking widths are actually in the range 1–20 $\times 10^{-3}$°. For inorganic crystals, the mosaic blocks can be directly seen *via* an electron microscope. So far, X-ray diffraction using a synchrotron beam is the only probe which has been used to reveal the presence of mosaic blocks in protein crystals *via* mosaicity measurements (Helliwell, 1988) and X-ray topography (Fourme *et al.*, 1995; Chayen *et al.*, 1996). As mentioned above, the focused laser beam is easily transmitted through the crystal thickness and might therefore encounter different mosaic blocks in its passage. Therefore, the effect of mosaicity should, in principle, interfere with the Raman data presented here. In Fig. 12 the relative intensity of the ggg S—S Raman line measured in the geometry where the polarizer and analyzer are parallel to each other and to the prism face of the TLSC (the *ZZ* and *YY* geometries are the specific cases) is presented as a function $I(\Delta\psi)$, $\Delta\psi$ being the rotation of the crystal as a whole around the X axis. This function has been simulated for tetragonal lysozyme on the basis of the PDB data (PDB code 193L). $\Delta\psi = 0^\circ$ corresponds to the *ZZ* geometry and $\Delta\psi = 90^\circ$ corresponds to the *YY* geometry. Fig. 12 shows that this function has a very small value of the first derivative both for the *ZZ* and *YY* geometries. This explains why the interference of the mosaicity on the data presented is negligible. In other words, it is impossible to detect the presence of the mosaic blocks in the present work.

Let us compare two tetragonal lysozyme crystals whose atomic coordinates are available in the PDB: earth-grown (code 193L) and space-grown (code 194L). The structural data derived from the PDB for these two crystals are presented in Table 3. Vaney *et al.* (1996) concluded that the space-grown crystal is slightly less ordered than the earth-grown crystal (1.33 *versus* 1.4 Å). The unusually high difference in θ_2 (1.13°) indeed indicates, according to the model derived from the Raman data described above, a better alignment of the protein molecules along the Z axis in the earth-grown crystal ($\theta_2^E = 25.14^\circ$) compared with the space-grown crystal ($\theta_2^S = 26.27^\circ$). The calculation gives the following values of ρ_{ggg} for these crystals: $\rho_{ggg}^E = 1.46$; $\rho_{ggg}^S = 1.42$. Thus, we

should notice differences between the polarized Raman spectra of the crystals. It is actually reasonable to propose that earth- and space-grown crystals (PDB codes 193L and 194L, respectively) have slightly different average orientations of the protein molecules within the crystal lattice, leading to a small difference in the value of the lattice constant a (78.54 and 78.65 Å, respectively). The presumption is that there exist shallow minima in the crystal free energy corresponding to relatively stable crystal structures of the same space group with slightly different lattice parameters. Each minimum probably corresponds to a specific orientation of the protein within the crystal lattice. This situation is unlikely for inorganic crystals, but could be possible for protein crystals built from large asymmetric soft molecules with complex surface structures, which allow the creation of a number of different intermolecular bonds.

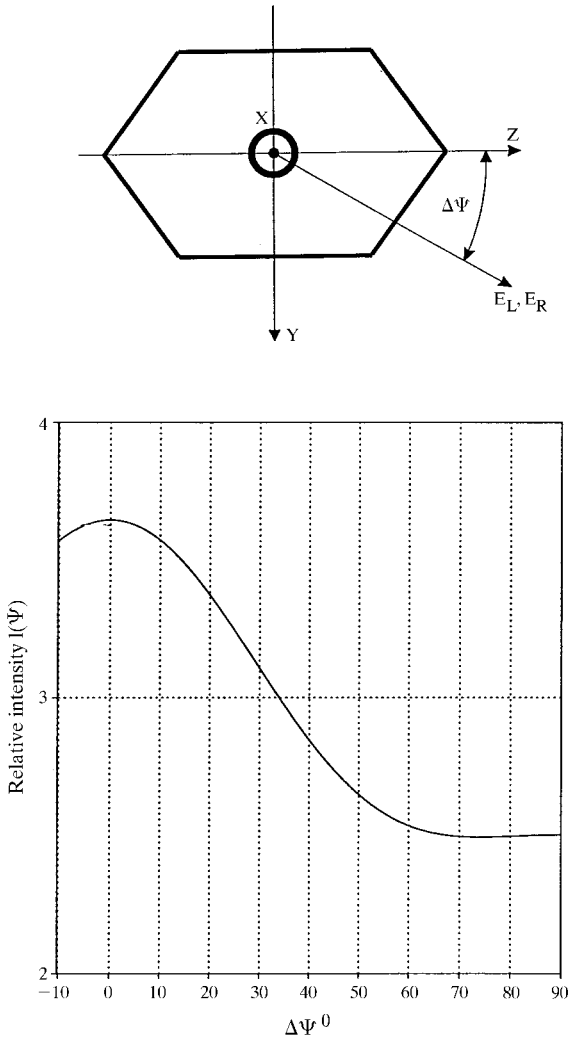

Fig. 12. Plot of $I(\Delta\psi)$ simulated for the TLSC (PDB code 193L). E_L, polarization of laser light; E_R, polarization of the analyzed Raman light.

According to this model, the mosaic blocks of protein crystals cannot achieve perfect orientational ordering of constituent molecules as in completely ideal crystals. In the protein case, the smearing of the diffraction reflection contours $I(\varphi)$ will correspond to variation in the orientation of the protein molecules within the lattice of each of the mosaic blocks. The strong variation of protein-crystal lattice constants with solution conditions, revealed by Thorne *et al.* (1997), would support such a hypothesis.

Returning to Fig. 12, it is worth mentioning that the first derivative of the function $I(\Delta\psi)$ reaches its maximum at $\Delta\psi = 30^\circ$. In such a geometry the angular misalignment of the mosaic blocks would, for instance, cause a maximum change in the intensity of the ggg S—S Raman line. Therefore, it seems promising to use this geometry to measure the Raman image of the tetragonal lysozyme prism faces in the spectral window from 502 to 512 cm^{-1}, corresponding to the ggg S—S Raman band, in the attempt to detect separate mosaic blocks in this image. This experiment could probably be accomplished by utilizing the DILOR XY Raman Microprobe system (Instruments SA Inc.) equipped with a confocal Raman imaging option (patented line-scan technique). The confocal option adds the third dimension to the image, making it as a real three-dimensional image with a spatial resolution of ~1 μm. We plan to perform such an experiment and our hope is to resolve the mosaic structure of TLSC in the Raman image, based on the high sensitivity and dynamic range of the CCD camera and on the relatively high intensity of the lysozyme ggg S—S Raman band. In addition, it should be possible to use the Raman technique in conjunction with diffuse scattering X-ray measurements from protein crystals to examine the effect of different crystal-growth methods on molecular-level disorder effects, and for different proteins.

In conclusion, we have shown that the Raman spectrum of TLSCs provides information consistent with the average orientation of protein molecules along the crystallographic fourfold axis, the extent of the perturbation of the proteins within the crystal lattice and the interlattice water content.

All of these effects can be interpreted as arising from structural features that collectively affect the quality of lysozyme crystals irrespective of the mosaic-block structure of a crystal.

The authors would like to thank Professor John Helliwell of the University of Manchester for many helpful e-mail discussions during the revision stage of this paper. The authors also wish to thank Dr Christie Brouillette for valuable remarks regarding the manuscript, Mr Randy Mann for performing the X-ray diffraction analysis and graduate students Candice Clary and Dan Crouthamel for their help in the preparation of this paper.

References

Blake, C. C. F., Mair, G. A., North, A. C. T., Phillips, D. C. & Sarma, V. R. (1967). *Proc. R. Soc. London Ser. B*, **167**, 365–377.

Carey, P. R. (1982). *Biochemical Applications of Raman and Resonance Raman Spectroscopies.* New York: Academic Press.

Chayen, N. E., Boggon, T. J., Cassetta, A., Deacon, A., Gleichmann, T., Habash, J., Harrop, S. J., Helliwell, J. R., Nieh, Y. P., Peterson, M. R., Raftery, J., Snell, E. H., Hädener, A., Niemann, A. C., Siddons, D. P., Stojanoff, V., Thompson, A. W., Ursby, T. & Wulff, M. (1996). *Q. Rev. Biophys.* **29**, 227–278.

Clarage, J. B., Clarage, M. S., Phillips, W. C., Sweet, R. M. & Caspar, D. L. D. (1992). *Proteins*, **12**, 145–157.

Fourme, R., Ducruix, M., Ries-Kautt, M. & Capelle, B. (1995). *J. Synchrotron Rad.* **2**, 136–142.

Genzel, L., Keilmann, F., Martin, T. P., Winterling, G. & Yacoby, Y. (1976). *Biopolymers*, **15**, 219–225.

Helliwell, J. R. (1988). *J. Cryst. Growth*, **90**, 259–272.

Imoto, T., Johnson, L. N., North, A. C. T., Phillips, D. C. & Rupley, J. A. (1972). *The Enzymes*, edited by P. Boyer, Vol. VII, pp. 666–869. New York: Academic Press.

Kachalova, G. S., Myachin, E. T., Morozov, V. N., Morozova, T. Ya., Vagin, A. A., Strokopytov, B. V. & Vol'kenstein, M. V. (1987). *Dokl. Biophys. (Engl. Transl.)* **293**, 236–238.

Lord, R. C. & Yu, N.-T. J. (1970). *J. Mol. Biol.* **50**, 509–524.

Nadarajah, A. & Pusey, M. (1996). *Acta Cryst.* D**52**, 983–996.

Sugeta, H., Akikatsu, G. & Miyazawa, T. (1972). *Chem. Lett.* 83–36.

Thorne, R. E., Dobrianov, I. & Finkelstein, K. D. (1997). *Bull. Am. Phys. Soc.* **42**, 820.

Tu, A. T. (1982). *Raman Spectroscopy in Biology: Principles and Applications.* New York: John Wiley & Sons.

Vaney, M. C., Maignan, S., Riès-Kautt, M. & Ducruix, A. (1996). *Acta Cryst.* D**52**, 505–517.

Wart, H. E. van, Lewis, A., Scheraga, H. A. & Saeva, F. D. (1973). *Proc. Natl Acad. Sci. USA*, **70**, 2619–2623.

Wilkinson, G. R. (1973). *The Raman Effect*, Vol. 2, *Applications*, edited by A. Anderson, pp. 408–579. New York: Marcel Dekker.

Yu, N.-T. & Jo, B. H. (1973). *Arch. Biochem. Biophys.* **156**, 469–474.